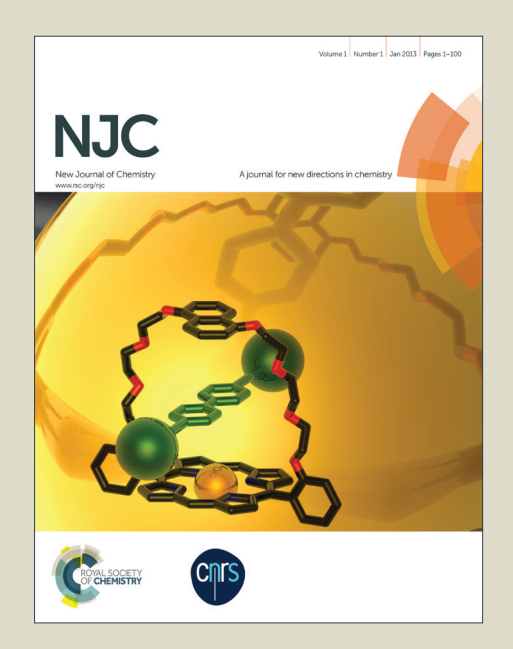
NJC

Accepted Manuscript



This is an *Accepted Manuscript*, which has been through the Royal Society of Chemistry peer review process and has been accepted for publication.

Accepted Manuscripts are published online shortly after acceptance, before technical editing, formatting and proof reading. Using this free service, authors can make their results available to the community, in citable form, before we publish the edited article. We will replace this Accepted Manuscript with the edited and formatted Advance Article as soon as it is available.

You can find more information about *Accepted Manuscripts* in the **Information for Authors**.

Please note that technical editing may introduce minor changes to the text and/or graphics, which may alter content. The journal's standard <u>Terms & Conditions</u> and the <u>Ethical guidelines</u> still apply. In no event shall the Royal Society of Chemistry be held responsible for any errors or omissions in this *Accepted Manuscript* or any consequences arising from the use of any information it contains.



Facile fabrication and enhanced gas sensing properties of In₂O₃ nanoparticles

Shuangming Wang, Pan Wang, Zhifang Li, Chuanhai Xiao, Bingxin Xiao, Rui Zhao, Tianye Yang and Mingzhe Zhang **

Received (in XXX, XXX) Xth XXXXXXXX 20XX, Accepted Xth XXXXXXXX 20XX DOI: 10.1039/b000000x

synthesized In₂S₃ nanoparticles and are developed for the detection of acetone gas. The In₂O₃ nanoparticles are characterized by TEM, HRTEM, SAED, EDX and XRD. Moreover, the products are further studied by room temperature UV-absorption and photoluminescence (PL) spectra. To demonstrate the usage of such nanoparticles, gas sensors based on the as-synthesized In₂O₃ nanoparticles are fabricated and exhibit good selectivity, high sensitivity, rapid response, low concentration detection limit and better repeatability to acetone gas at a relatively low operating temperature. Such excellent gas sensing performances are attributed to small crystal sizes and the existence of abundant oxygen vacancies. As demonstrated, the single crystalline In₂O₃ nanoparticles are highly promising for real-time monitoring gas sensor applications.

1. Introduction

With the stepwise improvement of our living standards, the 15 environment issues, especially air pollution, are becoming more and more serious. In order to effectively detect toxic and combustible gases, significant efforts have been focused on exploring functional materials, which can be applied in fabricating high sensitive gas sensors with excellent gas sensing 20 performances. 1,2 In₂O₃, as an n-type wide band gap semiconductor, has been acknowledged as a promising candidate for practical gas sensing application due to the high conductivity and abundant defects both in the sensing body and on the surface.3 Until to now, various morphologies of In₂O₃ with 25 different dimensional nanostructures, such as nanoparticles, 4 nanowires, ⁵ nanotubes, ⁶ thin films ⁷ and complicated hierarchical structures constructed with nanoscale building block, have been synthesized. It can be easily found that for the most of these synthesis methods, In₂O₃ are fabricated by annealing the as-30 prepared precursors, 9-11 such as In(OH)3, InOOH and In₂S₃. And these synthetic methods usually require the high temperature, the sophisticated equipment or complex procedures. Furthermore, in comparison with In(OH)₃ and InOOH, In₂S₃ is less reported as the precursor of In₂O₃, but has attracted more and more attention 35 due to its promising applications in optical, photoconductive and optoelectronic fields. 12 In addition, it is noteworthy that there are no reports on In₂S₃ gas sensing properties until now.

Among the preparation methods of In₂S₃ nanomaterials, the solution-phase route is regarded as an economic alternative way with the advances of being low-cost, mild, and more controllable in the reaction process. However, regardless of all the advantages

of the solution phase synthetic strategies in producing nanomaterials, it is still a challenge to find more routes, which are simpler and easier because these factors are crucial to further industrial application. Hence, on the basis of the above, the fabrication of In₂O₃ nanomaterials by exploring more simple and effective techniques is highly desirable.

In this work, In₂O₃ nanocrystals with sizes of 10-40 nm have been successfully fabricated by annealing as-prepared In₂S₃ so nanoparticles precursors for the first time. And In₂S₃ is synthesized via a simple and facile gas-liquid phase chemical deposition method at room temperature from common and low-cost In(COOCH₃)₃·3H₂O, Na₂S and hydrochloric acid. The as-obtained In₂O₃ nanoparticles are developed for the detection of acetone gas and their sensing properties have been investigated in detail. The gas sensing tests indicate the sensors based on the assynthesized In₂O₃ nanoparticles exhibit superior gas sensing performances towards acetone gas at a relatively low operating temperature, demonstrating their feasible applications in the sensor devices.

2. Experimental section

2.1 Fabrication of In₂S₃ and In₂O₃ nanoparticles

All the reagents (analytical-grade purity) were used as purchased without further purification. Deionized water was used in the experiments. The experimental set-up and steps can be found in our previous report. In a typical synthesis process, 3 mmol In(COOCH₃)₃·3H₂O and 3 mmol HOCH₂CH₂SH was dissolved to 300 mL and 50 mL deionized water under stirring to form a uniform transparent solution, respectively. Subsequently, the two solutions were mixed together to obtain the reactive solution,

whose pH value was adjusted to 3.8-4.0 by the ethylic acid. And then the reactive solution was transferred into the reaction chamber with circulating water (25 °C), which was placed in an ultrasonic bath to avoid particles agglomeration and promote the 5 new liquid surface emerging that then reacted with the flowing H₂S gas. H₂S gas prepared by adding 1 mol/L hydrochloric acid to 1 mol/L sodium sulfide aqueous solution was taken into the chamber by the flow of nitrogen to participate in the synthesis process. In the beginning, numerous nuclei was formed and 10 started to grow on gas-liquid interface. Under the effect of ultrasound, the particle dispersed into the solution, and the new liquid surface emerged. This process was repeated until the reaction was fully completed. The precipitates were collected by centrifugation, washed several times with deionized water and 15 absolute alcohol, respectively, and then dried in a nitrogen atmosphere.

The final yellowish In_2O_3 nanoparticles were obtained by calcining the as-prepared precursors (In_2S_3 nanoparticles) at 600 $^{\circ}$ C for 3 h in air. The heating rate was controlled at 1 $^{\circ}$ C/min.

20 2.2 Characterization

Transmission electron microscopy (TEM), high resolution transmission electron microscopy (HRTEM) and selected area electron diffraction (SAED) images were obtained on a JEOL JEM-2200FS microscope operated at 200 kV. The crystal phases of the synthesized samples were characterized by X-ray powder diffraction (XRD), which was conducted on a Rigaku D/max-2500 X-ray diffractometer with Cu Kα (λ=0.15418 nm). An energy-dispersive X-ray spectroscope (EDX) equipped in the JEOL JSM-6700F field emission scanning electron microscope (FESEM) was used to determine sample compositions. Room temperature UV–vis absorption spectrum and PL spectrum was recorded on UV-3150 spectrophotometer (Japan, Shimadzu) and a violet diode laser with the excitation wavelength of 405 nm, a spot size of 20 μm and a power of 30 mW, respectively.

35 2.3 Fabrication of gas sensors

The as-prepared In_2O_3 (0.01 g) nanomaterials were uniformly dispersed into distilled water (about 0.1 mL) to form a paste. Then the paste was painted on the surface of a ceramic tube (outer diameter = 1.35 mm, length = 4 mm) on which a pair of gold electrodes was previously printed. A Ni-Cr heating wire (diameter = 0.5 mm, resistance = 35 Ω) was inserted into the tube to heat the gas sensor directly. In order to improve their stability and repeatability, the gas sensors were sintered at 350 °C for 10 h

in air.

The sensor was welded on a socket and the electrical properties of the sensor were measured by a CGS-8 intelligent gas sensing analysis system. The sensor response was defined as $S = R_a/R_g$. Here, R_a and R_g were the resistances of the sensors in the air and target gas, respectively. The response and recovery time was defined as the time taken by the sensors to achieve 90% of the total resistance change in the case of adsorption and desorption, respectively.

3. Results and discussion

 ${\rm In_2O_3}$ nanoparticles are successfully fabricated by annealing asprepared ${\rm In_2S_3}$ nanoparticles precursors (synthesized via a facile gas-liquid phase chemical deposition route at room temperature). The as-obtained ${\rm In_2O_3}$ nanoparticles are developed for a gas sensor and exhibit an excellent acetone gas sensing performance.

3.1 Morphology and composition analysis

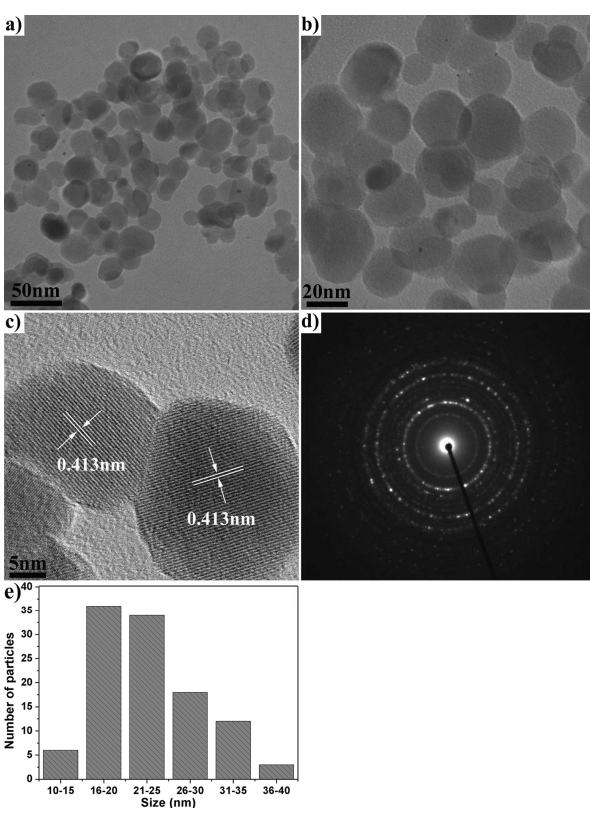


Fig. 1 (a) the low-magnification, (b) the enlarged and (c) the high-magnification TEM image, (d) the SAED pattern and (e) particles size distribution plot of In₂O₃ nanoparticles, respectively. The morphology, structure and particle size of the samples are investigated by TEM images. As demonstrated in Fig. S1, the precursors are In₂S₃ nanoparticles, which are identical with our previous reports. ^{13,14} As shown in Fig. 1, after the annealing treatment, the In₂O₃ nanoparticles are obtained and the particles

become near spherical and edge-clear. Fig. 1a, 1b and 1c present the typical TEM images of In₂O₃ nanoparticles at different magnifications. The low magnification TEM image (Fig. 1a and 1b) clearly show that the product is composed of a large number 5 of irregular nanoparticles. No other morphologies can be observed, indicating the high uniformity of the as-obtained products. Meanwhile, it is also found that the obtained In₂O₃ nanoparticles show slight agglomeration. Similar phenomenons have also been reported in the earlier literatures. 15,16 A typical 10 HRTEM image (Fig. 1c) of two nanoparticles clearly exhibits the lattice fringes of pure In₂O₃. The fringes from the continuous lattice structure confirm that the nanoparticle is a single crystal. Lattice fringes spaced by 0.413 nm correspond to In₂O₃ (211) lattice planes. As shown in Fig. 1d, the selected-area electron 15 diffraction (SAED) image reveals distinct diffraction rings, indicating polycrystalline structure of the In₂O₃ nanoparticle products. Furthermore, a sample of 110 imaged particles is measured from different TEM images in order to calculate the mean particle size and obtain a size distribution (Fig. 1e). All 20 particles imaged are smaller than 40 nm and a relatively broad distribution (10-40 nm) is observed compared with the calculated mean particle diameter of 23 nm.

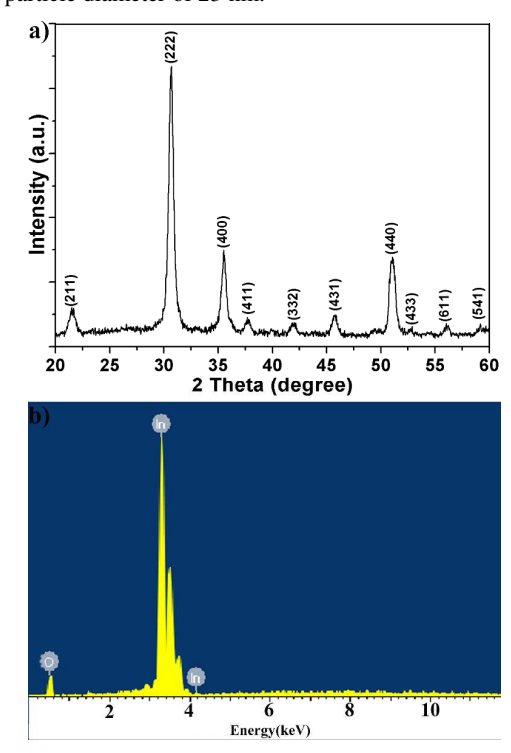


Fig. 2 The XRD pattern and EDX spectrum of In_2O_3 nanoparticles

The crystal phase of the In_2O_3 product is characterized by XRD. The typical XRD pattern of the In_2O_3 nanoparticles is shown in

Fig. 2a. All of the diffraction peaks can be well indexed to the standard In₂O₃ (JCPDS No. 71-2195). No diffraction peaks from any other impurities are observed. In addition, the EDX spectrum (Fig. 2b) is performed to further obtain chemical composition of the as-prepared In₂O₃ nanoparticles. The result confirms that the present In₂O₃ nanoparticles contain only In and O, without the contamination of S, indicating a complete transformation from ³⁵ In₂S₃ to In₂O₃.

3.2 UV-vis and PL spectra

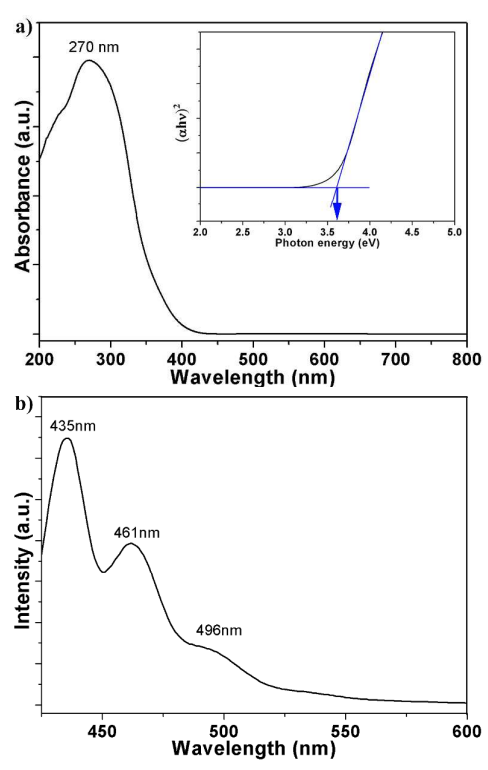


Fig. 3 The room temperature (a) UV-visible absorption spectrum and (b) PL spectrum of In_2O_3 nanoparticles. The inset of (a) is the ${}_{40}$ plot of $(\alpha hv)^2$ versus hv

As a promising transparent conducting oxide material, the ultraviolet-visible light absorption spectrum of as-prepared In₂O₃ nanoparticles has been further clarified and shown in Fig. 3a. The absorption spectrum is obtained by the measurement of the In₂O₃ samples in the reflection mode. After the conversion, the absorption spectrum is presented. The result indicates that In₂O₃ nanoparticles exhibit absorption peaked at about 270 nm in the ultraviolet region. And the corresponding plot of $(ahv)^2$ vs hv for the as-prepared In₂O₃ is presented in the inset of Fig. 3a. The band gap energy E_g for the In₂O₃ samples can be determined by extrapolation to the zero absorption coefficient. ^{17,18} As shown in the inset of Fig. 3a, the intercept of the tangent to the plot will give a good approximation of the band gap energy. Extrapolation

of linear portion to the energy axis at $(ahv)^2 = 0$ gives the E_g value. The band gap for the as-prepared In_2O_3 is determined to be about 3.6 eV. Moreover, the absorption study obviously indicates that In_2O_3 nanoparticles are transparent in the visible region.

In order to investigate any correlations between the structure of samples and their responses towards exposed gases, room temperature PL characteristics of nanoparticles are also studied and shown in Fig. 3b. A strong emission peak is centered at 435 nm, and two shoulders appear at 461 and 496 nm. The strong 10 peak centered at 435 nm is located in the blue light region. And the blue luminescence emission mechanism of In₂O₃ is mainly attributed to the existence of oxygen vacancies, 19,20 which is very beneficial to the enhancement of the gas sensing performances. 21,22 Generally, the emission spectra can be divided 15 into two broad categories: the near-band emissions and the deeplevel emissions, in which the former can be favored by the high crystal quality and quantum confinement effect and the latter can be enhanced by impurities, low crystallinity or structural defects of the crystals. Due to the high temperature annealing process, the 20 existence of various levels produced oxygen vacancies become the predominant factor to PL emission. 23, 24

3.3 Acetone sensing properties

Acetone, as a common reagent, is widely used in industries and labs, and is harmful to human health and safety. Inhalation of ²⁵ acetone can cause headache, fatigue and even narcosis and harmfulness to nerve system. ²⁵ Hence, the detection of acetone is of great importance and much needed for both environmental protection and human health. For this reason we fabricate an n-type semiconductor gas sensor based on the as-prepared In₂O₃ nanoparticles and investigate its gas sensing performances toward acetone gas.

In the gas sensing study, the operating temperature is important for the investigation on gas sensing properties due to its great influence on the surface state of sensing materials, as well as the contact reactions during the gas sensing process. To investigate the influence of the operating temperature and to get an optimum operating temperature of the sensors, the sensing responses of the In₂O₃ sensor to 50 ppm acetone as a function of operating temperature are tested and the results are shown in Fig. 4a. Obviously, the response of the sensor is highly dependent on the operating temperature. And the sensitivities of the present In₂O₃ nanomaterials are found to increase on increasing the operating temperature, attain the maximum, and then decrease on further

increasing the operating temperature. This decrease in the response at high temperatures may be attributed to the decrease in the number of active sites for the adsorption of acetone. Another possibility is that at such high temperatures, the rate of adsorption is lower than that of desorption.³ The maximum response value is obtained at the operating temperature of 240 °C, which is lower than the results of the literatures.²⁶⁻²⁹ Therefore, the optimal operating temperature of 240 °C is chosen for acetone to further examine the characteristics of the sensor.

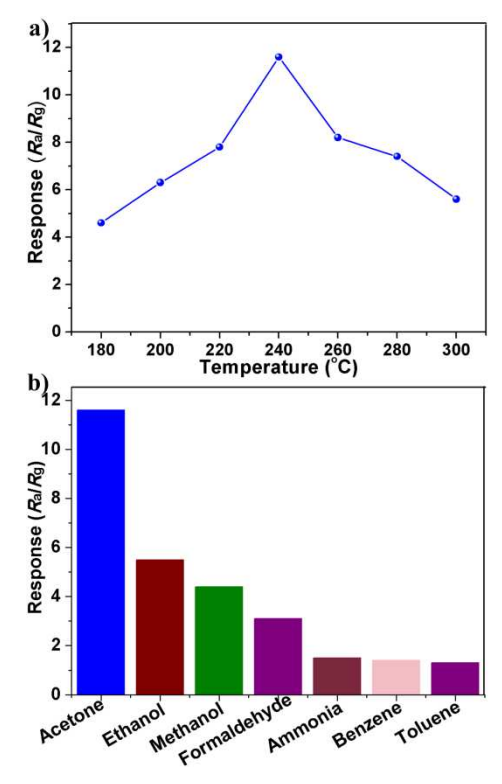


Fig. 4 (a) Response of the sensor based on In_2O_3 nanoparticles to 50 ppm acetone as a function of operating temperature; (b) the response of the In_2O_3 based sensor to 50 ppm different test gases at 240 °C.

The gas sensing selectivity is another parameter to evaluate the sensing ability of semiconductor materials. Fig. 4b exhibits the response of the In₂O₃ sensor at 240 °C to 50 ppm various test gases. The result indicates that the sensor shows the highest response to acetone (11.6), lower responses to ethanol, methanol and formaldelyde and is almost insensitive to ammonia, benzene and toluene. The sensor exhibits a higher response to acetone than to other gases, which is mainly attributed to the enhanced reaction between the acetone and the absorbed oxygen at the optimum operating temperature.

The dependence of sensitivity on acetone concentration is measured and shown in Fig. 5. In the low concentration range from 1 to 50 ppm (the inset of Fig. 5), the sensitivity near linearly increases with increasing the acetone concentration. And the response of the sensor rapidly increases with increasing acetone concentration until 500 ppm. Above 500 ppm, the sensitivity slowly changes with the variations of the acetone concentration, which indicates that the sensor becomes more or less saturated.

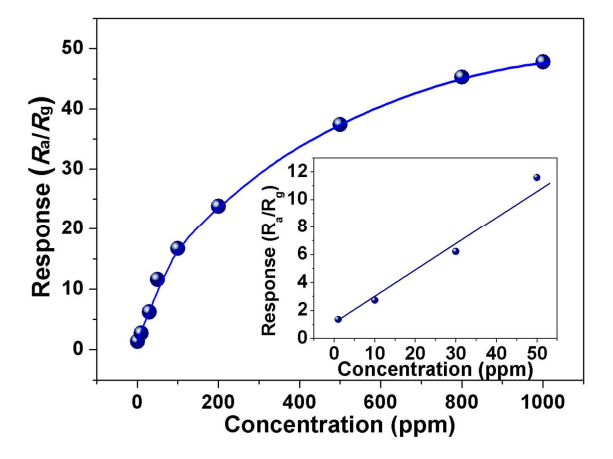


Fig. 5 Responses of the In_2O_3 sensor to different concentrations of acetone at 240 $^{\circ}C$.

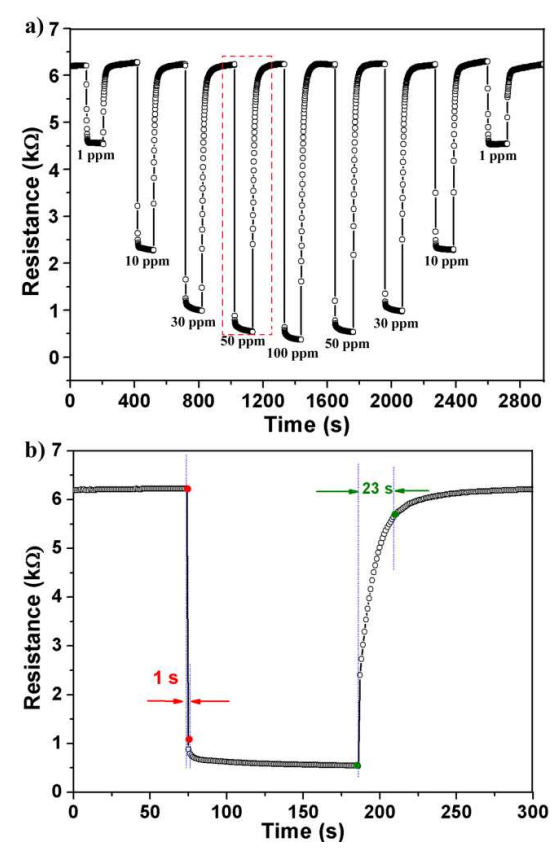


Fig. 6 The dynamic response of the In_2O_3 nanoparticles based sensors to different acetone concentrations (1-100 ppm) at 240 °C, (b) the response transient of the In_2O_3 based sensors to 50 ppm acetone at 240 °C.

Fig. 6a shows the dynamic responses of the In₂O₃ nanoparticles based sensors to different concentrations (1-100 ppm) of acetone gas at 240 °C. It is apparent that the sensor has a wide detection range from 1 ppm to 100 ppm. In addition, the responses of the sensor change rapidly on being exposed to acetone and to air, 20 indicating the excellent reproducibility of the sensors, and the asfabricated sensor shows a clear and fast response change when exposed to the concentration of acetone as low as 1 ppm with a response value of about 1.4. For a gas sensor, the response and recovery time are also very important parameters, which are 25 demanded for practical application. Fig. 6b shows the typical response transient of the In₂O₃ nanoparticles based sensor when it is exposed to 50 ppm acetone gas. The results indicate that the sensor immediately responds when acetone gas is introduced and then rapidly recovers to its initial value after the acetone is 30 released. The response time and recovery time is calculated to be ~ 1 s and ~ 23 s, respectively.

Table 1 The performance of acetone gas sensors based on various nanostructures in the literatures and In_2O_3 nanoparticles in this study (DL: detection limit)

Sample	Acetone (ppm)	S	t _{res} /t _{rec} (s)	DL (ppm)	T(°C)	Ref
In ₂ O ₃ nanowire	25	7	-/-	-	400	5
La ₂ O ₃ -doped ZnO	10	7.6	9/13	-	350	26
Ni-doped SnO ₂ nanofiber	50	46.2	7/30	-	340	28
In ₂ O ₃ hollow spheres	100	~ 8	8/15	-	300	29
Ce-doped SnO ₂ sphere	100	11.9	18/7	-	250	30
Mesoporous Fe ₂ O ₃	50	4.7	1.7/76	0.5	240	31
WO ₃ nanoplate	50	~8	5/10	2	300	32
In ₂ O ₃ nanospheres	30	~11	-/-	-	200	33
Au-loaded NiO hybrid structure	50	10.2	-/-	5	240	34
In ₂ O ₃ nanoparticles	50	11.6	1/23	1	240	This work

A comparison between the sensing performances of the In₂O₃ nanoparticles based sensor and literature reports is summarized in Table 1. It is noteworthy that although the response value of the sensor based on pure In₂O₃ nanoparticles is not the highest, the ⁴⁰ optimum working temperature (240 °C) is lower than some

literature reports. $^{5,26,28-30,32}$ In addition, the rapid response time (1 s), recovery time (23 s) and low detection limit (1ppm) also show the advantage of pure In_2O_3 nanoparticles.

3.4 Gas sensing mechanism

- s Most semiconductor oxide gas sensors operate on the basis of modification of the electrical properties of an active element, which is brought about by the adsorption of an analyte on the surface of the sensor. 33,35,36 It is well-known that oxygen sorption plays a vital role in the electrical transport properties of In₂O₃ nanomaterials. In air, oxygen molecules can be adsorbed on the In₂O₃ nanoparticles to form O₂[−], O[−], O^{2−} ions by capturing electrons from the conductance band (O[−] is believed to be dominant at 240 °C), which increases the sensor resistance. While the In₂O₃ nanoparticles are exposed to a reductive gas, for example acetone, acetone molecules react with the adsorbed O[−], releasing the trapped electrons back to the conductance band, and then the resistance of the sensor decreases. The possible reaction of acetone with the adsorbed oxygen can be explained as follows: CH₃COCH₃ + 9O[−] (ad) → 3CO₂ + 3H₂O + 9e[−]. 34
- The enhanced gas sensing performances should be ascribed to two aspects. The first is that the as-prepared In₂O₃ nanoparticles present small crystal sizes (10-40 nm), which can strongly improve gas sensing performances. That is because that small crystals possess larger surface/volume ratio and thus provide more surfaces to interact with the target gas than big crystals. The second aspect for such excellent gas sensing properties can be attributed to the existence of abundant oxygen vacancies. As demonstrated in the PL spectrum, In₂O₃ nanoparticles own abundant oxygen vacancies, which can provide high energetic sites to further enhance the interaction between acetone molecules and In₂O₃ nanoparticles. Therefore, In₂O₃ nanoparticles fabricated in our work by a facile route can be developed to be acetone gas sensor in practice.

4. Conclusions

35 In summary, single crystal In₂O₃ nanoparticles with sizes of 10-40 nm have successfully been synthesized by annealing asprepared In₂S₃ precursors. The as-synthesized In₂O₃ nanocrystals exhibit superior acetone gas sensing performances in aspects of good selectivity, high sensitivity, fast response time, low detection limit and better repeatability at a relatively low working temperature, which are ascribed to small crystal sizes and the existence of abundant oxygen vacancies. The current work clearly demonstrates that our synthesized In₂O₃ nanoparticles can be

promisingly developed to be high performance acetone gas ⁴⁵ sensors in future.

Acknowledgements

This work was funded by the National Science Foundation of China, Nos. 11174103 and 90923032 and Specialized Research Fund for the Doctoral Program of Higher Education of China, No. 20130061110012.

Notes and references

State Key Laboratory of Superhard Materials, Jilin University, Changchun 130012, People's Republic of China. * E-mail address: zhangmz@jlu.edu.cn.

- 55 1 N. V. Long, Y. Yang, M. Yuasa, C. M. Thi, Y. Q. Cao, T. Nann and M. Nogami, *RSC advances*, 2014, 4, 8250.
- 2 X. Z. Wang, S. Qiu, C. Z. He, G. X. Lu, W. Liu and J. R. Liu, *RSC advances*, 2013, **3**, 19002.
- 3 X. M. Xu, X. Li, W. B. Wang, B. Wang, P. Sun, Y. F. Sun and G. Y. Lu, *RSC advances*, 2014, **4**, 4831.
- 4 Z. H. Li, Y. Li, Y. X. Luan, J. C. Li and A. X. Song, *CrystEngComm*, 2013, **15**, 1706.
- 5 A. Vomiero, S. Bianchi, E. Comini, G. Faglia, M. Ferroni, N. Poli and G. Sberveglieri, *Thin Solid Films*, 2007, **515**, 8356.
- 65 6 J. Liu, W. Li, L. H. Zhu, C. Li, F. D. Qu, W. B. Guo, C. H. Feng, S. P. Ruan, J. Nanosci. Nanotechno., 2014, 14, 3653.
 - 7 M. Hellwig, H. Parala, J. Cybinksa, D. Barreca, A. Gasparotto, B. Niermann, H. W. Becker, D. Rogalla, J. Feydt, S. Irsen, A. V. Mudring, J. Winter, R. A. Fischer and A. Devi, *J. Nanosci*.
- 70 Nanotechno., 2011, 11, 8094.
 - 8 X. M. Xu, P. L. Zhu, D. W. Wang, P. Sun, L. You, Y. F. Sun, X. S. Liang, F. M. Liu, H. Chen and G. Y. Lu, *Sens. Actuators, B*, 2013, 176, 405.
- 9 P. Song, D. Han, H. H. Zhang, J. Li, Z. X. Yang and Q. Wang,
- s Sens. Actuators, B, 2014, **196**, 434.
- 10 B. L. Tao, Y. Zhang, D. Z. Han, Y. P. Li and Z. F. Yan, *J. Mater. Chem. A*, 2014, **2**, 5455.
- 11 L. N. Zhang, W. Zhang, H. B. Yang, W. Y. Fu, W. Y. Zhao, H. Zhao and J. W. Ma, *Mater. Chem. Phys.*, 2011, **130**, 932.
- 80 12 B. Chai, P. Zeng, X. H. Zhang, J. Mao, L. Zan and T. Y. Peng, Nanoscale, 2012, 4, 2372.
 - 13 B. B. Yao, H. Y. Zhu, S. M. Wang, P. Wang and M. Z. Zhang, J. Solid State Chem., 2014, 210, 150.
- 14 B. B. Yao, P. Wang, S. M. Wang and M. Z. Zhang,
- 85 CrystEngComm, 2014, 16, 2584.
 - 15 T. Ould-Ely, D. Prieto-Centurion, I. Rusakova and K. H.

- Whitmire, CrystEngComm, 2013, 15, 6918.
- 16 J. Q. Xu, X. H. Wang and J. N. Shen, Sens. Actuators, B, 2006, 115, 642.
- 17 S. M. Wang, J. Y. Liu, G. L. Cui, B. B. Yao and M. Z. Zhang,
- 5 Mater. Lett., 2013, 94, 186.
 - 18 Y. Zeng, T. Zhang, L. J. Wang, R. Wang, W. Y. Fu and H. B. Yang, J. Phys. Chem. C, 2009, 113, 3442.
- 19 H. X. Yang, L. Liu, H. Liang, J. J. Wei and Y. Z. Yang, CrystEngComm, 2011, 13, 5011.
- 10 20 L. N. Jin, Q. Liu and W. Y. Sun, Mater. Lett., 2013, 102, 112.
- 21 S. M. Wang, P. Wang, C. H. Xiao, B. B. Yao R. Zhao and M. Z. Zhang, *CrystEngComm*, 2013, **15**, 9170.
- 22 Y. Zeng, T. Zhang, L. J. Wang, R. Wang, W. Y. Fu and H. B. Yang, *J. Phys. Chem. C*, 2009, **113**, 3442.
- 15 23 H. Zhu, X. L. Wang, L. Qian, F. Yang and X. R. Yang, J. Phys. Chem. C, 2008, 112, 4486.
 - 24 C. L. Chen, D. R. Chen, X. L. Jiao and S. H. Chen, J. Phys. Chem. C, 2007, 111, 18039.
 - 25 P. Song, Q. Wang and Z. X. Yang, Mater. Lett., 2012, 86, 168.
- 20 26 J. Q. He, J. Yin, D. Liu, L. X. Zhang, F. S. Cai and L. J. Bie, Sens. Actuators, B, 2013, 182, 170.
 - 27 X. J. Wang, W. Wang and Y. L. Liu, *Sens. Actuators*, *B*, 2012, **168**, 39.
 - 28 J. P. Cheng, B. B. Wang, M. G. Zhao, F. Liu and X. B. Zhang,
- 25 Sens. Actuators, B, 2014, 190, 78.
- 29 D. Han, P. Song, H. H. Zhang, Z. X. Yang and Q. Wang, *Mater. Lett.*, 2014, **124**, 93.
- 30 P. Song, Q. Wang and Z. X. Yang, *Sens. Actuators*, B, 2012, **173**, 839.
- 30 31 X. H. Sun, H. M. Ji, X. L. Li, S. Cai and C. M. Zheng, J. Alloys. Comp., 2014, 600, 111.
 - 32 D. L. Chen, X. X. Hou, T. Li, L. Yin, B. B. Fan, H. L. Wang, X. J. Li, H. L. Xu, H. X. Lu, R. Zhang and J. Sun, Sens. Actuators, B, 2011, 153, 373.
- 35 33 Z. Guo, J. Y. Liu, Y. Jia, X. Chen, F. L. Meng, M. Q. Li and J. H. Liu, Nanotechnology, 2008, 19, 345704.
 - 34 L. L. Wang, Z. Lou, T. Fei and T. Zhang, *Sens. Actuators, B*, 2012, **161**, 178.
 - 35 R. Li, J. M. Du, Y. X. Luan, H. Zou, G. S. Zhuang and Z. H. Li,
- 40 CrystEngComm, 2012, 14, 3404.
 - 36 J. Cao, T. Zhang, F. Li, H. Yang and S. Liu, *New J. Chem.*, 2013, **37**, 2031.
 - 37 J. M. Ma, J. Zhang, S. R. Wang, Q. H. Wang, L. F. Jiao, J. Q.

- Yang, X. C. Duan, Z. F. Liu, J. B. Lian and W. J. Zheng, *CrystEngComm*, 2011, **13**, 6077.
- 38 R. Li, Y. X. Luan, H. Zou, J. M. Du, T. C. Mu and Z. H. Li, *RSC advances*, 2012, **2**, 3049.
- 39 S. Elouali, L. G. Bloor, R. Binions, I. P. Parkin, C. J. Carmalt and J. A. Darr, *Langmuir*, 2012, 28, 1879.
- 50 40 C. H. Chen, Y. L. Wei, D. R. Chen and X. L. Jiao, *Mater. Chem. Phys.*, 2011, **125**, 299.
- 41 D. Wang, J. B. Sun, X. Cao, Y. H. Zhu, Q. X. Wang, G. C. Wang, Y. Han, G. Y. Lu, G. S. Pang and S. H. Feng, *J. Mater. Chem. A*, 2013, 1, 8653.
- 55 42 M. Kaur, N. Jain, K. Sharma, S. Bhattacharya, M. Roy, A. K. Tyagi, S. K. Gupta, J. V. Yakhmi, *Sens. Actuators, B*, 2008, **133**, 456.
- 43 M. Epifani, J.D. Prades, E. Comini, E. Pellicer, M. Avella, P. Siciliano, G. Faglia, A. Cirera, R. Scotti, F. Morazzoni, J.R.
- Morante, J. Phys. Chem. C, 2008, **112**, 19540.